Buffer amplifier to connect the SG-056 to a Q330HR recording system

Thomas Forbriger
Black Forest Observatory (BFO)
Heubach 206, D-77709 Wolfach

2011-09-15

Contents

List of Tables

List of Figures

1 Purpose

The superconducting gravimeter SG 056 at BFO shall be recorded on a seismic data acquisition system additionally to the usual SG-datastream recorded with DVMs (digital voltmeters). A Q330HR (Kinemetrics, Inc.) data acquisitions system will be installed for this purpose and the second output of the SG gravity cards will be supplied to this digitizer. The Q330HR expects to receive symmetric differential input signals while the SG 056 superconducting gravimeter electronics just supply single ended signals. The buffer amplifier produces symmetric output signals to be recorded on the Q330HR.

We further plan to increase the bandwidth of this data stream by getting rid of the GGP low-pass filter. On the SG gravity card an alternative signal path via the GWR low-pass filter is present. Since the corner period of this low-pass still is at 5s, we plan to modify its corner frequency or to get rid of it entirely. Since the SG feedback loop does not contain any low-pass filter, strong ultra-high frequency signals (up to a few Megahertz) are present at the lock-in output. For this reason the buffer amplifier to the Q330HR should contain a moderate low-pass.

2 Circuit description

The circuit diagram is presented in Fig. 2 and the specification for the components are listed in Tab. 1. The board layout, component placement and wiring are apparent in Figs. 3, 4, and 5, respectively.

Three channels will be passed to the Q330HR:

CH1: The gravimeter signal of sensor G1

CH2: The gravimeter signal of sensor G2

CH3: The FBM-signal (feedback modulator) which is used for calibration of the instrument's frequency response

Identical buffer amplifiers are provided for each of the signals. The first stage (IC1) is a low-pass filter in a modified Sallen-Key design (GWR uses this low-pass filter design). The filter properties are specified in Figs. 6 and 7. The second stage (IC2) is a simple inverter providing the symmetric output signal.

The signal cable from the buffer amplifier to the Q330HR puts a capacitive load of approx. 270 pF on the output of the amplifier. Together with the finite output resistance of the operational amplifiers, this makes the feedback ineffective at some high frequency, resulting in strong HF-oscillations of the operational amplifiers. To compensate for this, a high-frequency by-pass feedback was introduced for both stages. The compensation solution is outlined by Horowitz and Hill (1980, Fig. 7.17). The corner frequency of the compensation is deliberately chosen to be in the kHz-range. This adds some additional low-pass property to the entire circuit, for the costs of non-symmetric behaviour at kHz frequencies and higher.

2.1 Wiring of connections to SG

Connector types and order codes are summarized in Tab. 2. Signal pins are specified in Tabs. 3, 4, 6, and 5.

2.1.1 Power supply connector

The power supply cable provides four wires: (1) +15 V analog (white), (2) +15 V common (red), (3) -15 V analog (green), and (4) -15 V common (black). On the circuit diagram for the *GEP3 POWER SUPPLY* (GWR. INST. B2000-028, 980316-S1, GEP3V1B.SCH) we find the *NOTE 1:*

> All DC outputs float from earth when exiting this chassis. Both analog COM and digital COM are referenced to earth (chassis ground) on the GEP3 back plane adjacent to the power input lines.

It therefore appears safe to tie +15 V common and -15 V common together in the power supply connector (Tab. 3). A pin diagram is shown in Fig. 1 (left).

2.1.2 Gravimeter signal connector

GWR supplies signal cables with an open end consisting of a blue and a white wire. The cable wiring diagram (dwg. no. GWR-GEP3-1651-509-02/03, Rev. A, 51-509.dwg) indicates connections as specified in Tab. 4. The circuit diagram for the *GRAVIMETER CONTROL CARD COMPONENT A1&A2 VERSION 4.00* (GWR. INST. B2000-028, 000828-S2, A1-V4-2B.SCH) defines the signal outputs as given in the lower table in Tab. 4. The output is protected by a surge suppressor diode. Connector P1 there is described as *high resolution data port, grav data 1, grav data 2*. Connector pins for the signals from the SG056 to the buffer amplifier are defined in Tab. 5. A pin diagram is shown in Fig. 1 (right). Connector pins for the signals from the buffer amplifier to the Q330HR are defined in Tab. 6.

2.2 Operational amplifier selection

We consider bipolar OpAmps like the OP27, OP07, and OP177. Generally it is difficult to obtain values for OpAmp noise at long-period seismic frequencies from data sheets. I refer to values at 1 Hz where available. The OP27 has extraordinary low voltage noise. Since we use 10 kΩ source resistors, the OP27 is no longer superior to the OP07. This is demonstrated in Figs. 5 and 6 in the OP27 data sheet (Analog Devices, 2003). The OPA627 has extremely low current noise, but becomes only superior to the OP27 at input source resistances larger than 10 kΩ (Burr Brown, 1998). The OP177 is only superior in terms of low offset and offset stability, not in terms of amplifier noise with respect to OP07 (Analog Devices, 2002b). Offset stability is an issue for long-period noise performance.

Currently the OP07 is selected for the buffer amplifier. The differenct variaties of OP07 differ slightly in noise characteristics, but by not more than a factor 2 (Analog Devices, 2002a).

3 Performance tests

During performance tests the Q330HR SN 4409 was used for data acquisition. For data production in the SG chamber a different Q330HR will be installed.

The Q330HR SN 4409 is equipped with six high-resolution channels with a nominal gain of

$$\frac{2^{26}}{40}\,\frac{\text{counts}}{\text{V}} = 1677721.6\,\frac{\text{counts}}{\text{V}}. \qquad (1)$$

Some of the results discussed below are attributed to the apparent signal of the SG056. I use the less sensitive sen-

sor G2 as a reference with a calibration factor (Geib, 2010) of

$$-80.07\,\frac{\mu\text{gal}}{\text{V}} \tag{2}$$

resulting in a conversion factor of

$$-47.73\,\frac{\text{pgal}}{\text{count}} = -47.73\cdot 10^{-12}\,\frac{\text{gal}}{\text{count}}. \tag{3}$$

For comparison the calibration factor of sensor G1 is

$$-40.11\,\frac{\mu\text{gal}}{\text{V}}. \tag{4}$$

3.1 Cross-talk

Significant non-linear low-frequency cross-talk was present without the compensation feedback in the OpAmp circuits. This was due to high-frequency oscillations presumably caused by the cable capacitance at the output which, together with the finite output resistance of the OpAmps, made the OpAmp feedback ineffective at high frequencies.

With the compensation feedback described in section 2 this problem disappeared. Even at input signal amplitudes of 10 V peak-to-peak, no cross-talk is apparent above noise level of the unused channels. The distance between the drive signal on one channel and the noise floor on the neighbouring channel is 140 dB. Tests were carried out on 29.11.2010.

3.2 Self-noise

Self-noise of the Q330HR (SN 4409) as well as of the buffer amplifier was studied in November 2010 in the BFO electronics laboratory. Noise conditions were worse than expected for the operation within the mine due to diurnal temperature variations, due to room heaters and due to possible electromagnetic interference with other equipment.

3.2.1 Q330HR self-noise

Q330HR (SN 4409) self-noise was recorded from 22.11.2010 until 26.11.2010 (time series duration: approximately 4 days). The Q330HR inputs were open and caps were placed on the connectors. The peak-to-peak amplitude of the diurnal signal was about 50–100 counts being equivalent to 30–60 μV or 2.5–5 ngal for the less sensitive sensor of the SG056 (G2 with 80 $\mu\text{gal}\,\text{V}^{-1}$). For signal periods smaller than 1000 s the broad-band peak-to-peak amplitude was about 6 counts being equivalent to 4 μVor 0.3 ngal. The spectral distribution of the noise-floor specified as signal rms in 1/6 decade is flat between 1 mHz and 200 mHz at the level of 0.008 ngal for sensor G2. It slightly raised about 20 dB up to 0.06 ngal at 50 Hz. At frequencies less than 1 mHz the noise level increased significantly to 1 ngal at 0.01 mHz. The latter should be attributed to the unfortunate thermal conditions during the test. These values are all the same for all six channels of the digitizer.

3.2.2 Buffer amplifier self-noise

With the buffer amplifier connected to channels 1–3 of the Q330HR and buffer amplifier inputs shorted, the self-noise only is slightly increased with respect to the Q330HR alone between 0.2 mHz and 50 Hz. The strongest increase was observed at 10 mHz, where the noise level was raised by 10 dB to about 0.03 ngal rms amplitude in 1/6 decade. From 0.01 mHz to 50 Hz the noise-floor was at least 40 dB below the NLNM (Peterson, 1993, New Low Noise Model) at all frequencies.

3.3 Linearity

Linearity was tested in December 2010. For the test a sinusoidal beating signal was produced by two synthesizers. The sinusoidal output of an HP 3325B synthesizer and a Toellner TOE 7405 function generator were mixed. The generator outputs were AC coupled via four 10 μF capacitors and mixed via four 2.7 kΩ resistors. For those tests where the signal was fed to the Q330HR directly, the signal was made symmetric with respect to Q330HR analog input GND by a voltage divider with two 8.2 kΩ resistors. As a carrier a 10 Hz sinusoidal signal was used in all cases. Two different beating frequencies were used, one being approximately 10 s, the other being approximately 3 s. This was necessary to distinguish the non-linear signal component from other harmonic noise components which appeared at the same level and must have been induced electromegnatically or being present in the noise-floor of the signal generators. The noise-floor of the signal generators appeared about 30–40 dB above the self-noise of the Q330HR and the buffer amplifier and limited the detection of harmonic components to a level of about 2–7 μV amplitude, which is about 120 dB below full drive.

With respect to linearity the first stage of the circuit with a non-inverting OpAmp design (Fig. 2) is not optimal. inverting OpAmp circuits avoid common mode signals at the OpAmp inputs and could be superior for this reason. The low-pass could be accomplished by a multiple feedback filter design with an inverting OpAmp stage. As a reference, the linearity of a simple combination of the inverting OpAmp used to produce a symmetric output signal, was tested too.

As a measure for non-linearity the amplitude of the intermodulation signals at the beating period were read from the low-pass filtered record. The results are listed in Tab. 7. In many cases an intermodulation signal could not be dected at all due to the noise-floor of the signal sources. In these cases the non-linear component of the output signal is at least less than $2 \cdot 10^{-6}$ of the full drive input signal. The worst case for the buffer amplifier was observed with an amplitude of the non-linear component of the output of $2 \cdot 10^{-6}$ of the drive signal. The overall worst case was observed for the simple amplifier of two inverting OpAmps with almost 10^{-5} of the carrier signal amplitude.

Apparently there is no reason to modify the filter stage of the circuit. Checking the data sheets and application notes of semiconductor manufacturers, it appears difficult to find any OpAmp which promises to behave better than 10^{-6} of non-linearity under optimal conditions.

3.4 Transfer function

On 10.2.2011 the transfer function of the final assembly was calibrated. A calibration of the buffer amplifier without the compensation feedback paths was done earlier, with results being presented in Tab. 8.

For the purpose of calibration a hand-made sweep signal was used containing harmonic components between 1 Hz and 100 Hz. The signal was kept at full drive amplitude of 20 V peak-to-peak at the amplifier output. The signal was swept from high frequencies to low frequencies and back again resulting in a smooth increase and decrease of amplitudes controlled by the decimation filter of the data acquisition system. The input signal was recorded via a simple amplifier of two inverting OpAmps on channel CH4 of the Q330HR as a reference. The test was analyzed using the program calex (Wielandt, 2002). Filter parameters were: 1) amplification, 2) eigenperiod T_0, 3) damping h as a fraction of critical damping, and 4) a constant delay. Results of tests with different initial parameters are listed in Tab. 9. The nominal values of the low-pass filter are

$$T_0 = 0.05\,\mathrm{s} \qquad \text{and} \qquad h = 0.866 \qquad (5)$$

and are matched remarkably well by the circuit parameters. The residuals of the time series simulated with the second order filter function are less than 10^{-4} of the input signal. The constant delay of 24 μs in all channels can safely be ignored in most cases.

When comparing the amplitude response of the nominal filter function to the spectral ratios between output and input signal, the residuals are less than 10^{-3} of the nominal gain for frequencies smaller than 2 Hz.

When testing the consistency within the buffer amplifier by fitting the output of one channel to the output of the other with a constant factor, the residual is smaller than 10^{-5} for a test frequency of approximately 60 s. Doing the same test with a broad-band sweep signal indicates that the residual mainly is due to a constant delay which differs by less than 0.1 ms between channels. This relatively strong apparent variation however is difficult to explain with respect to the results in Tab. 9.

3.5 DC gain

The DC gain was calibrated on 11.2.2011. DC test signals were applied to the inputs of the Q330HR on one hand and to the buffer amplifier on the other hand. The signal was made symmetric to analog GND by a resistive voltage divider when calibrating the Q330HR. The input voltages were stable to the level of $\pm 1 \cdot 10^{-5}$ with respect to the DC voltage. DC voltages were produced by a Philips reference voltage source and were controlled by an HP 3478A precision voltmeter. The accuracy of the HP 3478A is specified to by $\pm 4 \cdot 10^{-5}$ of the reading ± 3 counts. This results in an overall accuracy of better than $\pm 1 \cdot 10^{-4}$ for the test signal. The results are presented in Tab. 10. The buffer amplifier does not contribute to the overall gain residual at a significant level when compared to the gain residuals of the Q330HR SN 4409 alone.

4 Operation

Since July 2011 the Q330HR (S/N 3840) is connected to the auxiliary GGP filter outputs of the SG-056. Data is recorded with a `seedlink` data acquisition system on host `gamma`. Amplitude conversion factors as determined by Rudolf Widmer-Schnidrig (internal report 9/2011) are given in Tab. 11.

Residuals between data recorded on the UIPC data acquisition system (digitized with Agilent 34420A DVMs) and the Q330HR from the same GGP filter outputs, are used for quality ccontrol. Observations are:

1. The centroid of the readings in the UIPC data stream actually takes place about 600 ms after the indicated time of sample. DVM integration time is 400 ms. Useful residuals are only obtained by introducing an appropriately tuned delay to the UIPC data stream.
2. Remaining residuals are at least 40 dB below the NLNM (Peterson, 1993). See Tab. 12.
3. If the FBM I/O connector of the GEP3 (Gravimeter Electronics Package) is connected to input #3 of the buffer amplifier, strong boxcar signals of 1 s and 1200 s period are present on channel 3. This is the

case even if the FBM is not operational. Unfortunately these signals also appear in the residuals of the gravimeter signals. The signals apparently are produced by the trigger system in the DAC3 (Data Acquisition Controler) of the SG-056. For this reason input #3 of the buffer amplifier is disconnected from the FBM I/O and terminated at the input. Additionally, the cable from the DAC3 Trig 4 output is disconnected at the GEP3 FBM trigger input.

4. If the buffer amplifier is operated from the GEP3 power supply, the noise level is raised by 10 dB for G1 and by 20 dB for G2 in comparison to levels given in Tab. 12. Further the 1200 s period signal (FBM trigger) shows up in the residuals even without connecting the FBM I/O connector to the buffer amplifier. For this reason the buffer amplifier is operated from an additional, fully isolated, linearly regulated ± 15 V power supply.

Grounding between SG-056 and buffer amplifier apparently is an issue because of the single-ended (ground referenced) signal connections from the gravity cards to the input #1 and #2 of the buffer amplifier. The interference with the 1 s and 1200 s period signals probably is due to the additional ground connections when connecting the FBM I/O or using the GEP3 power supply.

Part #	Parameters
R1	10 kΩ, 0.1 %, TK 25 ppm
R2	10 kΩ, 0.1 %, TK 25 ppm
R3	20 kΩ
R4	10 kΩ, 0.1 %, TK 25 ppm
R5	10 kΩ, 0.1 %, TK 25 ppm
R6	5 kΩ
R7	100 Ω
R8	100 Ω
R9	100 Ω
R10	100 Ω
C1	689 nF, selected
C2	919 nF, selected
C3	4.7 nF, selected
C4	4.7 nF, selected
Cb	100 nF
Cs	220 μF
IC1, IC2	OP07 or better

Table 1: Components

References

Analog Devices, 2002a. OP07: Ultralow Offset Voltage Operational Amplifiers. Data Sheet DEV.A.

Analog Devices, 2002b. OP177: Ultraprecision Operational Amplifier. Data Sheet DEV.C.

Analog Devices, 2003. OP27: Low-Noise, Precision Operational Amplifier. Data Sheet DEV.C.

Burr Brown, 1998. OPA 627, OPA637: Precision High-Speed Difet Operational Amplifiers. Texas Instruments. Data Sheet, 2005.

Geib T., 2010. Genauigkeit der in-situ Kalibrierung des supraleitenden Gravimeters SG-056 am BFO. Diplomarbeit, Karlsruhe Institute of Technology (KIT), Geophysical Institute, Germany.

Horowitz P. and Hill W., 1980. The art of electronics. Cambridge University Press, Cambridge.

Peterson J., 1993. Observations and modeling of background seismic noise. Open-file report 93-322, U.S. Geological Survey, Albuquerque, New Mexico. <http://earthquake.usgs.gov/regional/asl/pubs/>.

Wielandt E., 2002. Seismic sensors and their calibration. In: P. Bormann (editor), *New Manual of Seismological Observatory Practice*, GeoForschungsZentrum, Potsdam, Germany. <http://www.software-for-seismometry.de>, doi:10.2312/GFZ.NMSOP_r1_ch5.

Connector	Type
cable connector for **G1 and G2 signals** at amplifier box	Bulgin 400 Series Buccaneer; PX0410/02S/5560 with sockets SA3349/1 http://www.bulgin.co.uk/Products/Buccaneer/Buccaneer_400_Series.html (PX0410/02S/4550 for 5mm cable diameter worked too)
sockets in amplifier box for **G1 and G2 signals**	Bulgin 400 Series Buccaneer; PX0412/02P with pins SA3350/1 http://www.bulgin.co.uk/Products/Buccaneer/Buccaneer_400_Series.html
cable connector amplifier box for **power supply**	Bulgin 400 Series Buccaneer; PX0410/04S/6065 with sockets SA3347/1
socket in amplifier box for **power supply**	Bulgin 400 Series Buccaneer; PX0412/04P with pins SA3348/1
socket in amplifier box for signals to Q330HR	Glenair 4907 IPT02A 12-8S F7 http://www.glenair.com/interconnects/commital/ipt/ipt_series.htm
cable to Q330HR at amplifier box	Glenair 0508 IPT06A 12-8P F7
cable to Q330HR at Q330HR sensor	CANNON-G KPT06F16-26P, with 26482-GR16-PG16D KPTC PG-Adapter; check for O-rings for the PG-Adapter, in some cases they must be ordered separately, O-rings from Cosy: 218554/10 TBF SCHRAUB D 21,9x1,8, Bezeichnung 980-8563-000; Kabelverschraubung: SKINTOP MS-SC 16, Art. Nr. 53112240, Lapp-Group, provided by Farnell: 53112240:Kabelverschraubung EMV PG1

Table 2: Connector types and order codes.

Figure 1: Buccaneer connector pin diagrams. Pins as seen in sockets in amplifier box when viewed from outside of box. Left: power supply connector. Right: Gravimeter signal connector.

pin	color	cable
1	white	+15V analog supply voltage
2	red	+15V common
3	green	-15V analog supply voltage
4	black	-15V common

Table 3: Power supply connector wiring. At cable: 400 Series Buccaneer PX0410/04S/6065 with sockets SA3347/1, at amplifier casing: 400 Series Buccaneer PX0412/04P with pins SA3348/1.

connector P1 at SG			open end at buffer amplifier		
pin	signal	wire	wire	label	amplifier input
3	DATA-2 HI	green	white	E3 FAST DIGITIZER HI	signal
4	DATA-2 LO	white	blue	E4 FAST DIGITIZER LO	ground

signal	pin	name of output
signal	P3-3	GRAV DATA 2 OUT A
AGND	P3-4	GRAV DATA 2 OUT B

Table 4: SG signal cable wiring. Upper table: G1 and G2 signal cable wiring as specified by GWR (dwg. no. GWR-GEP3-1651-509-02/03, Rev. A, 51-509.dwg). Lower table: output specification for gravity control card (GWR. INST. B2000-028, 000828-S2, A1-V4-2B.SCH).

pin	cable
1	signal
2	GND

Table 5: G1 and G2 signal connector wiring

Q330HR sensor conenctor			amplifier	
pin	STS-2 equivalent signal	wire	pin	signal
A	CH1+, Z+	brown	B	CH1+
B	CH1-, Z-	white (brown)	C	CH1-
C	CH1 GND	shield (brown)		NC
D	CH2+, N+	yellow	F	CH2+
E	CH2-, N-	white (yellow)	E	CH2-
F	CH2 GND	shield (yellow)		NC
G	CH3+, E+	green	G	CH3+
H	CH3-, E-	white (green)	A	CH3-
J	CH3 GND	shield (green)		NC
N	MposRTN A/B, GNDS	grey + white (grey)	D	GND
a	PGP, overall shield	shield	H	metal casing

Table 6: Signal connection to Q330HR. Signals and connector pin assignment at buffer amplifier end and Q330HR sensor connector.

channel	test	beating	carrier	intermodulation	non-linearity	comment
CH1	BufAmp	$\approx 10\,\mathrm{s}$	$\approx 8\mathrm{V}$	$< 8\,\mu\mathrm{V}$	$< 10^{-6}$	not detected
CH1	BufAmp	$\approx 3\,\mathrm{s}$	$\approx 8\mathrm{V}$	$\approx 15\,\mu\mathrm{V}$	$\approx 2 \cdot 10^{-6}$	
CH2&3	BufAmp	$\approx 13\,\mathrm{s}$	$\approx 8\mathrm{V}$	$< 10\,\mu\mathrm{V}$	$< 1.5 \cdot 10^{-6}$	not detected
CH2&3	BufAmp	$\approx 2.5\,\mathrm{s}$	$\approx 8\mathrm{V}$	$\approx 12\,\mu\mathrm{V}$	$\approx 1.5 \cdot 10^{-6}$	
CH6	Q330HR	$\approx 13\,\mathrm{s}$	$\approx 7\mathrm{V}$	$< 2\,\mu\mathrm{V}$	$< 10^{-6}$	not detected
CH6	Q330HR	$\approx 3\,\mathrm{s}$	$\approx 7\mathrm{V}$	$< 1.3\,\mu\mathrm{V}$	$< 10^{-6}$	not detected
CH4	SymAmp	$\approx 2.5\,\mathrm{s}$	$\approx 8\mathrm{V}$	$\approx 60\,\mu\mathrm{V}$	$\approx 8 \cdot 10^{-6}$	
CH4	SymAmp	$\approx 2.5\,\mathrm{s}$	$\approx 0.8\mathrm{V}$	$< 1\,\mu\mathrm{V}$	$< 1.5 \cdot 10^{-6}$	not detected

Table 7: Linearity test by measuring the intermodulation amplitude observed at the beating period of the input signal. BufAmp: Test of buffer amplifier channels. Q330HR: Test of Q330HR directly with out external amplifier as a reference. SymAmp: Test of a simple amplifier of two inverting OpAmps as a reference. Due to the noise-floor of the signal sources, an intermodulation not in all cases an intermodulation signal could be detected. The carrier signal always was a sinusoidal at 10 Hz. beating: beating period, i.e. amplitude modulation period. carrier: amplitude of the carrier drive signal (10 Hz signal). intermodulation: amplitude of the intermodulation signal at the beating period. non-linearity: amplitude of the intermodulation signal with respect to the amplitude of the carrier signal.

	initial		final		fixed
CH#	T_0 / s	h	T_0 / s	h	delay / ms
1	0.03	0.966	0.04995	0.8682	-0.4
1	0.03	0.666	0.04996	0.8681	-0.4
1	0.15	0.666	0.04996	0.8681	-0.4
1	0.15	0.666	0.04993	0.8684	0.0
2	0.02	0.966	0.04994	0.8684	-0.4
2	0.15	0.666	0.04995	0.8682	-0.4
2	0.15	0.966	0.04994	0.8683	-0.4
3	0.10	0.566	0.04996	0.8673	-0.8
3	0.10	0.966	0.04997	0.8671	-0.8
3	0.03	0.966	0.04995	0.8675	-0.8
3	0.03	0.966	0.04893	0.8682	-0.0

Table 8: Calibration of preliminary buffer amplifier low-pass (24.2.2010). Notice that these results might be biased due to undetected high-frequency oscillations of the buffer amplifier. The board was equipped with OP07DP. The signal used is a square wave of 20 V peak-to-peak amplitude. An additional negative signal delay was introduced, which significantly reduced the transient edge-response in the residual. Overall the largest residuals are at the level of 10 mV peak-to-peak. The additional delay times are significantly smaller than the signal delay due to the low-pass, which is about 14 ms. The cause for the additional delay is unclear. It could be due to a symmetric buffer that was used to record the calibration input signal.

	initial		final			
CH#	T_0 / s	h	T_0 / s	h	delay / μs	residual rms
1	0.01	0.566	0.05005	0.8670	24	$83 \cdot 10^{-6}$
1	0.11	0.566	0.05006	0.8670	24	$83 \cdot 10^{-6}$
1	0.31	1.266	0.05006	0.8670	24	$83 \cdot 10^{-6}$
2	0.01	0.566	0.05004	0.8674	24	$95 \cdot 10^{-6}$
2	0.11	0.566	0.05003	0.8674	25	$95 \cdot 10^{-6}$
2	0.11	1.566	0.05003	0.8674	24	$95 \cdot 10^{-6}$
3	0.01	0.566	0.05027	0.8666	24	$77 \cdot 10^{-6}$
3	0.11	0.566	0.05029	0.8666	24	$77 \cdot 10^{-6}$
3	0.31	1.266	0.05029	0.8666	24	$77 \cdot 10^{-6}$

Table 9: Calibration of buffer amplifier transfer function (10.2.2011). The test signal used is a sweeped sine wave of 20 V peak-to-peak amplitude at the amplifier output. Harmonic components between 1 Hz and 100 Hz are present in the sweep. Overall the largest residuals are at the level of 2 mV peak-to-peak, i.e. $\cdot 10^{-4}$ of the drive signal maximum. initial: Initial system parameters. The initial frequency independent signal deplay was zero in all cases. final: Final system parameters, providing the best least-squares fit for the synthetic output signal to the recorded output signal. residual rms: rms value of the residual signal with respect to the recorded signal.

channel	gain / counts V^{-1}	residual	internal precision	offset / V
CH1	$3.35584 \cdot 10^6$	$+1.2 \cdot 10^{-4}$	$1.7 \cdot 10^{-6}$	$-2.5 \cdot 10^{-4}$
CH1	$3.35592 \cdot 10^6$	$+1.4 \cdot 10^{-4}$	$1.9 \cdot 10^{-6}$	$-2.5 \cdot 10^{-4}$
CH2	$3.35789 \cdot 10^6$	$+7.3 \cdot 10^{-4}$	$1.7 \cdot 10^{-6}$	$-3.7 \cdot 10^{-4}$
CH2	$3.35798 \cdot 10^6$	$+7.5 \cdot 10^{-4}$	$2.3 \cdot 10^{-6}$	$+0.020 \cdot 10^{-4}$
CH3	$3.35636 \cdot 10^6$	$+2.7 \cdot 10^{-4}$	$1.7 \cdot 10^{-6}$	$-0.17 \cdot 10^{-4}$
CH3	$3.35645 \cdot 10^6$	$+3.0 \cdot 10^{-4}$	$2.0 \cdot 10^{-6}$	$-0.12 \cdot 10^{-4}$

channel	gain / counts V^{-1}	residual	internal precision	offset / V	common mode rejection
CH1	$1.67807 \cdot 10^6$	$+2.1 \cdot 10^{-4}$	$5.8 \cdot 10^{-6}$	$-4.1 \cdot 10^{-4}$	$1.4 \cdot 10^4$
CH2	$1.67891 \cdot 10^6$	$+7.1 \cdot 10^{-4}$	$5.8 \cdot 10^{-6}$	$-2.0 \cdot 10^{-4}$	$0.79 \cdot 10^4$
CH3	$1.67769 \cdot 10^6$	$-0.2 \cdot 10^{-4}$	$5.8 \cdot 10^{-6}$	$+1.5 \cdot 10^{-4}$	$0.94 \cdot 10^4$

Table 10: DC gain calibration. The upper table presents the results for the calibration of the buffer amplifier recorded on the Q330HR SN 4409. For each channels two readings were taken. The first reading was taken at $\pm 5\,V$ and the second at $\pm 0.5\,V$. The nominal DC gain is $2^{27} \cdot 40^{-1}\,\text{counts}\,V^{-1} = 3.3554432 \cdot 10^6\,\text{counts}\,V^{-1}$. As a reference the Q330HR SN 4409 was calibrated without the buffer amplifier. Readings were taken at $\pm 5\,V$. The results are presented in the lower table. The buffer amplifier does not contribute to the overall gain residual at a significant level. gain: DC gain as derived from calibration recording. residual: Residual of derived gain with respect to nominal gain as a fraction of nominal gain. internal precision: Precision of the derived gain value estimated from signal noise level. The actual accuracy is worse and depends on the accuracy of the reference voltmeter (see text). offset: Constant DC offset present in recorded data. common mode rejection: Reciprocal of: recorded common mode signal as a fraction of input common mode signal.

Q330HR	SG-056	conversion	comment
CH1, ?G1	sensor 1 (G1), lower	$-8.370762 \cdot 10^{12}$ counts $s^2\ m^{-1}$	
	and heavier sphere	$-0.119463 \cdot 10^{-12}\ m\ s^{-2}$ counts^{-1}	
CH2, ?G2	sensor 2 (G1), upper	$-4.194237 \cdot 10^{12}$ counts $s^2\ m^{-1}$	
	and lighter sphere	$-0.238422 \cdot 10^{-12}\ m\ s^{-2}$ counts^{-1}	
CH3, ?X3	FBM I/O		to be connected only upon request

Table 11: Connections established between Q330HR (S/N 3840) and SG-056. In Q330HR channel names, the question mark has to be replaced by H for 100 sps, B for 40 sps, and L for 1 sps.

Sensor	rms in 1/6 decade / nm s^{-2}	PSD / $nm^2\,s^{-4}\,Hz^{-1}$
G1	$7 \cdot 10^{-5} - 1 \cdot 10^{-4}$	$3 \cdot 10^{-6} - 1 \cdot 10^{-4}$
G2	$1 \cdot 10^{-4} - 2 \cdot 10^{-4}$	$1 \cdot 10^{-5} - 1 \cdot 10^{-4}$

Table 12: Remaining residuals between UIPC recording and Q330HR recording from same signal source in the frequency band 0.1 mHz to 50 mHz. Residuals are at least 40 dB below NLNM.

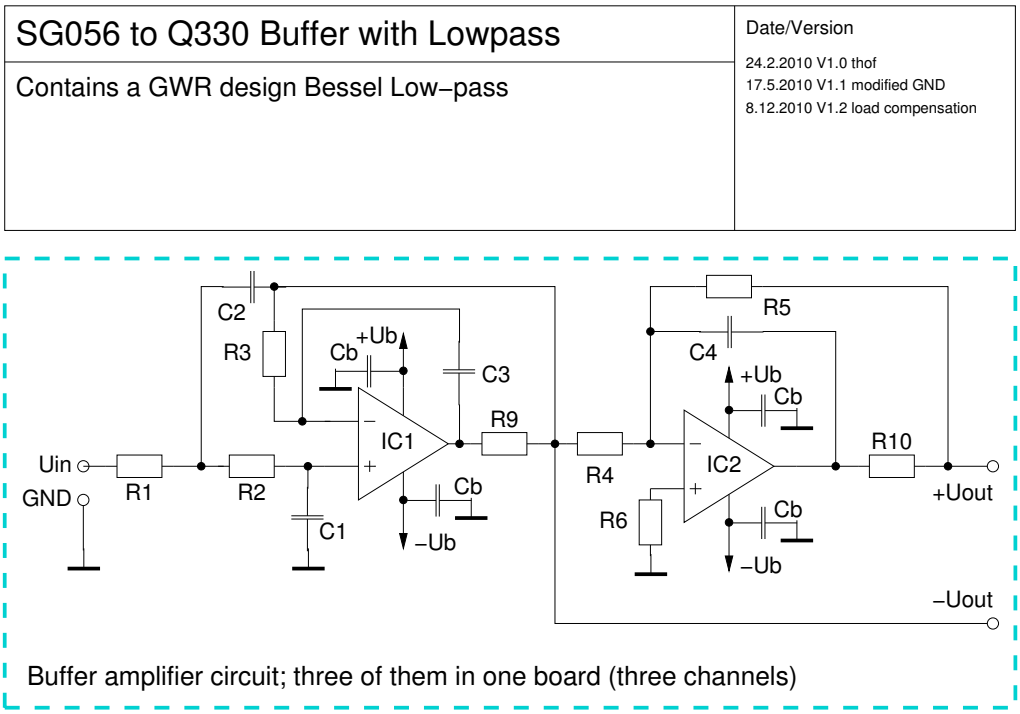

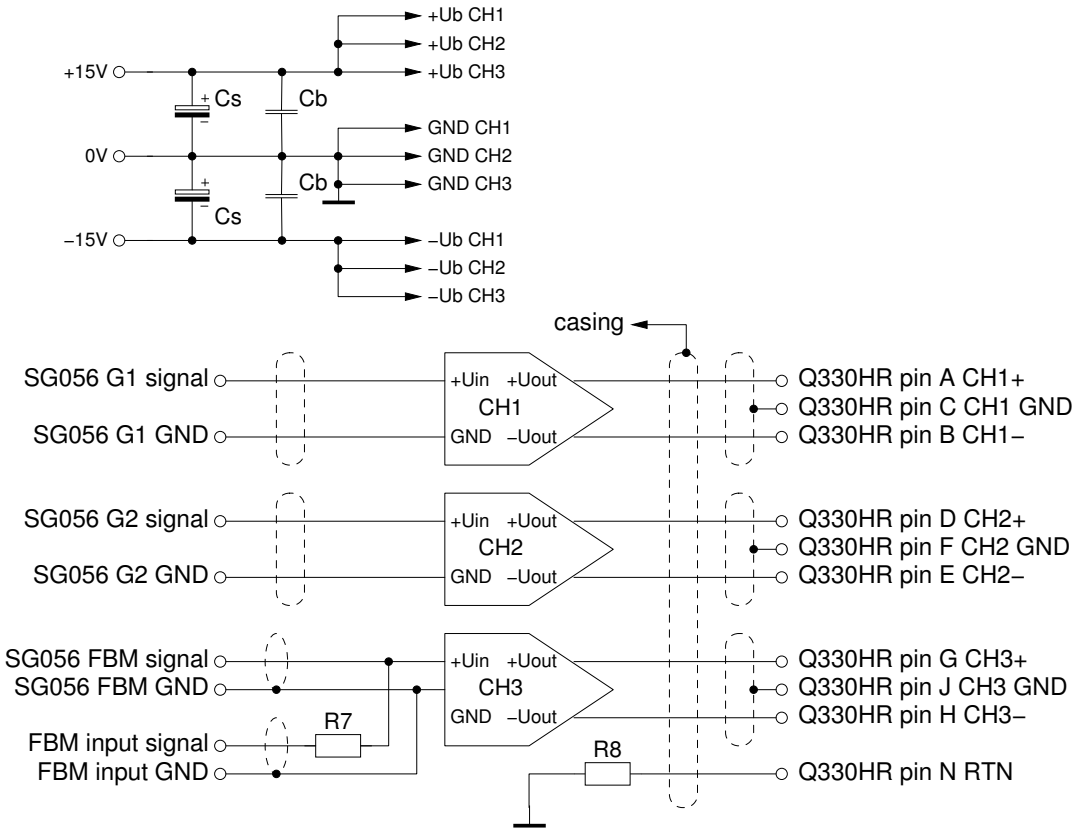

Figure 2: SG buffer amplifier with low-pass: Circuit diagram.

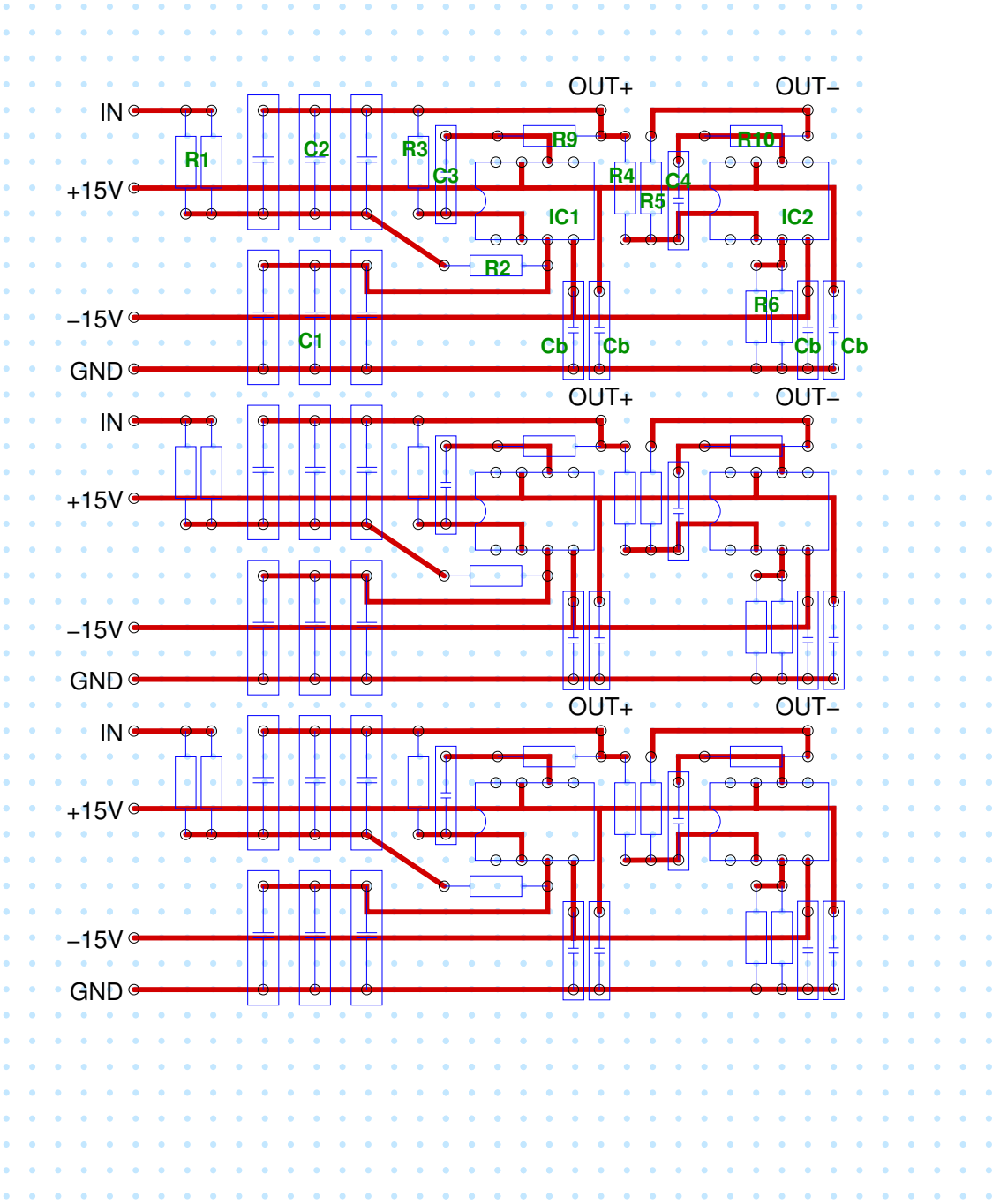

Figure 3: SG buffer amplifier with low-pass: Board layout.

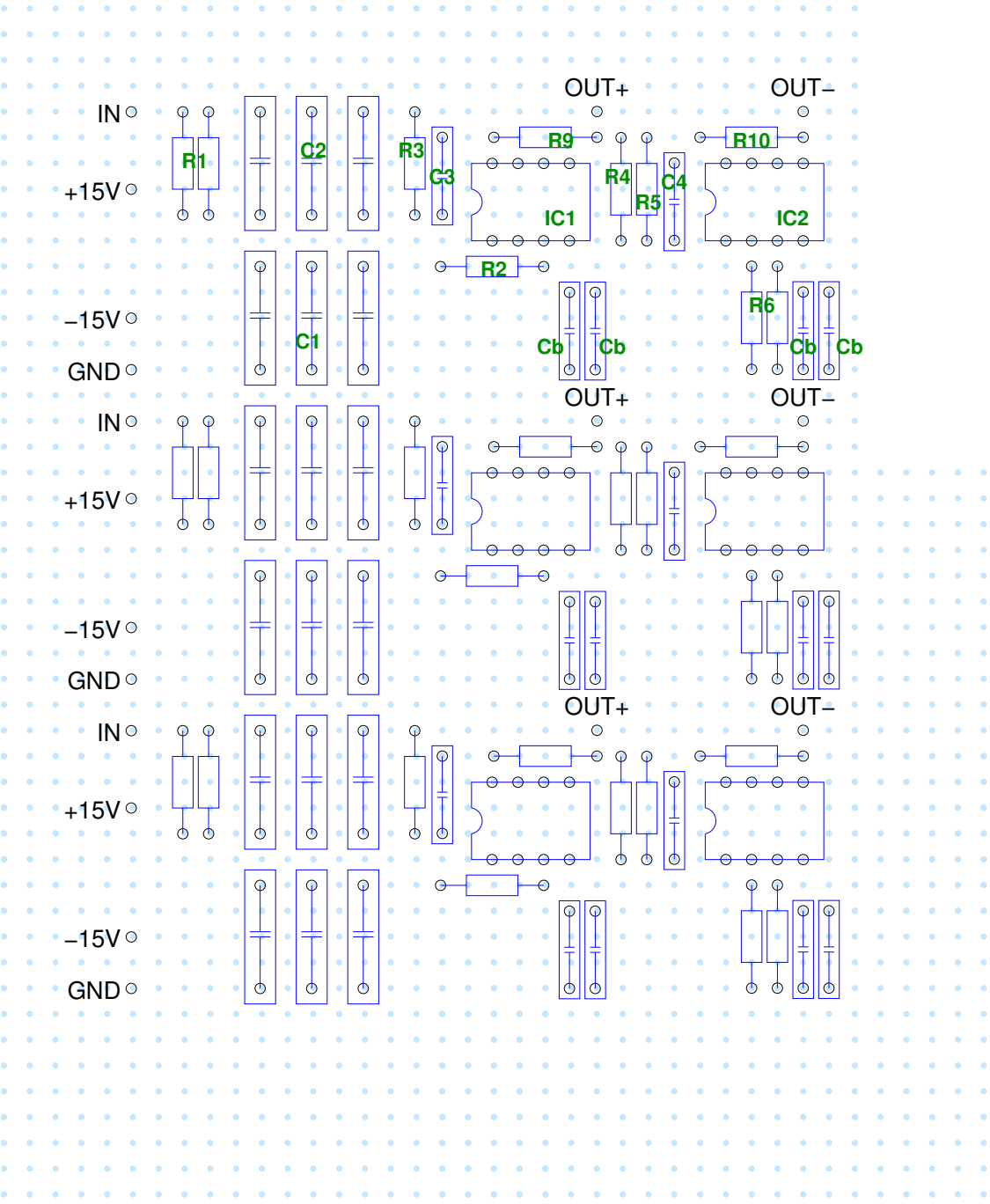

Figure 4: SG buffer amplifier with low-pass: Board layout component placement.

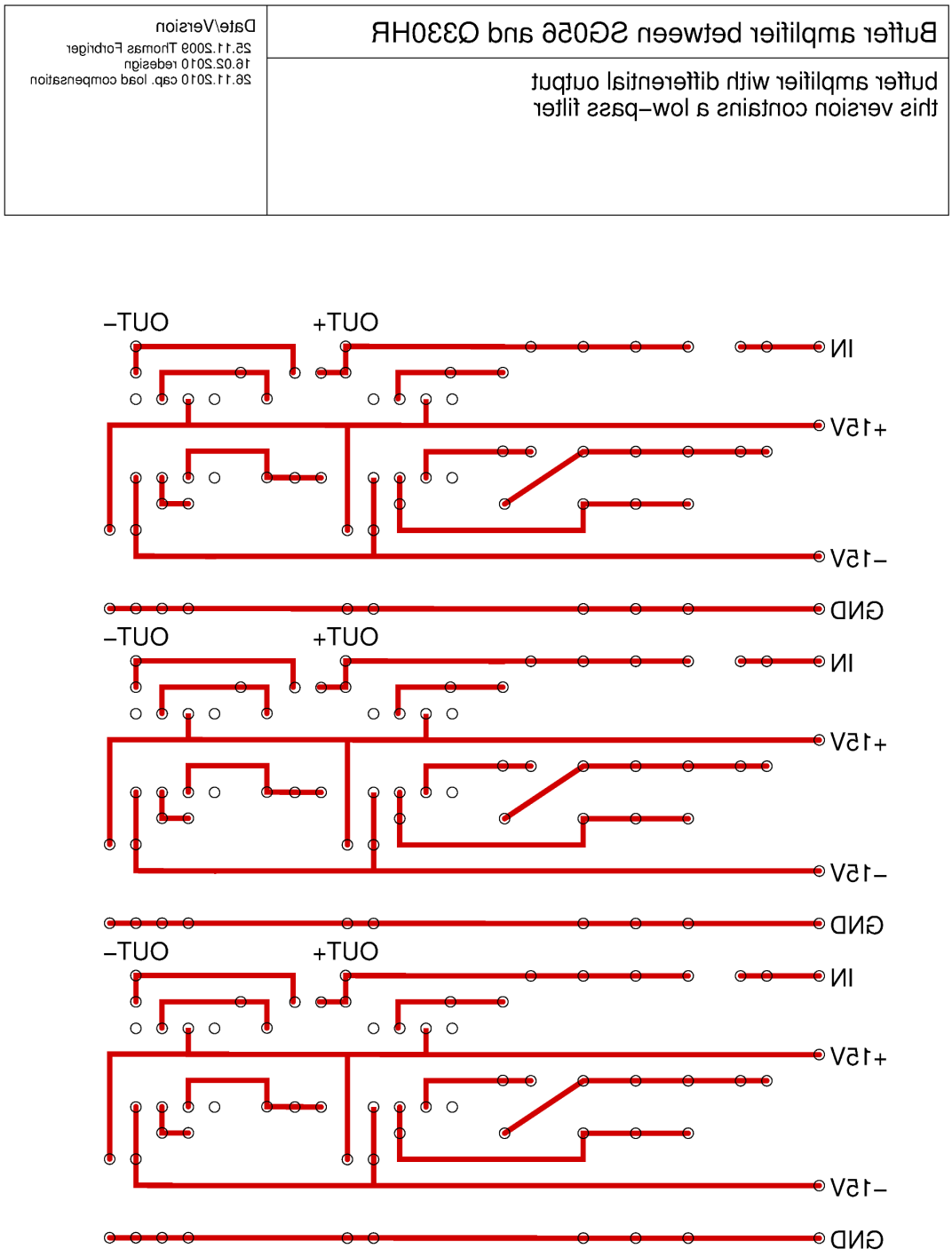

Figure 5: SG buffer amplifier with low-pass: Board layout wiring diagram.

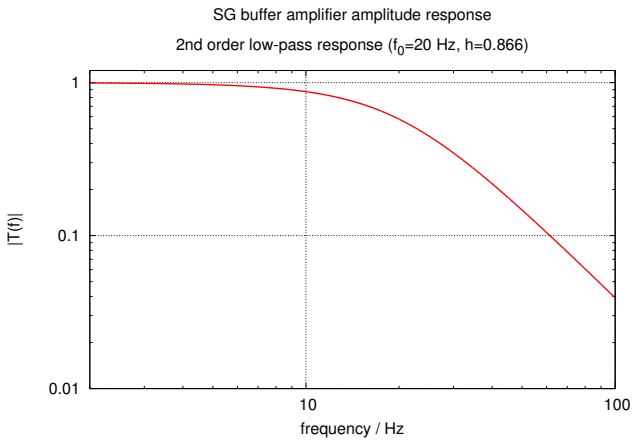

Figure 6: SG buffer amplifier with low-pass: Nominal filter amplitude response.

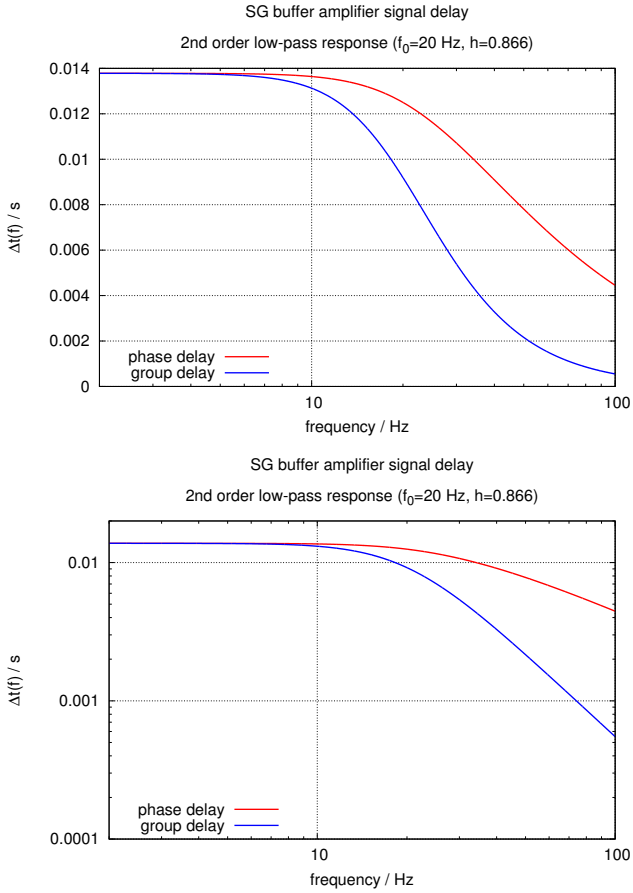

Figure 7: SG buffer amplifier with low-pass: Nominal filter delay.

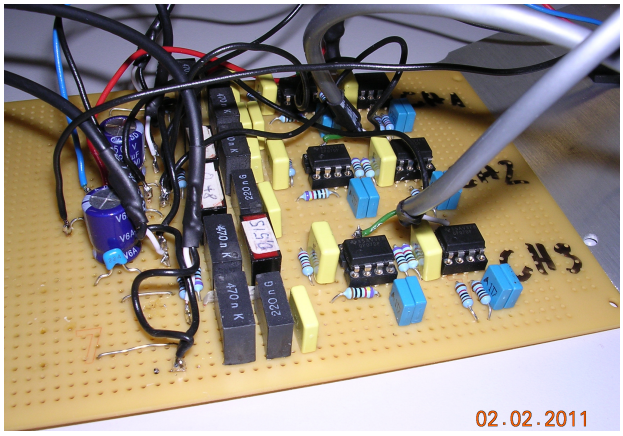

Figure 9: Picture of buffer amplifier board: component side.

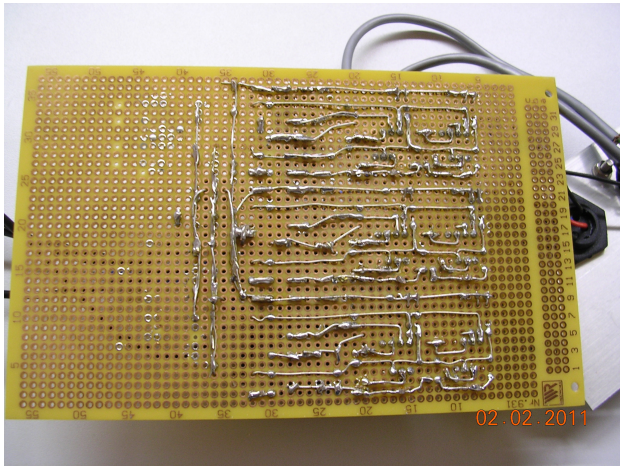

Figure 10: Picture of buffer amplifier board: solder side.

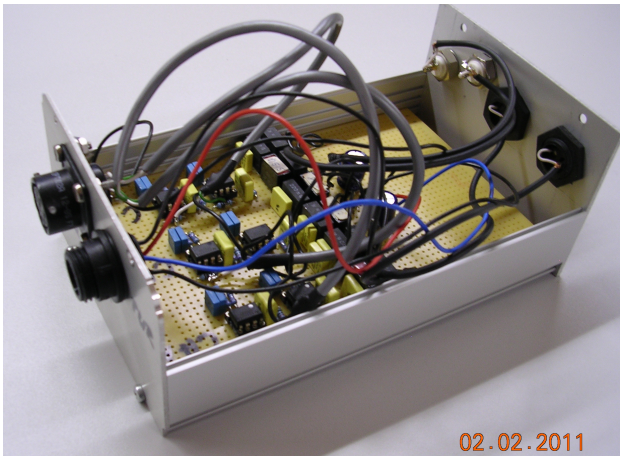

Figure 11: Picture of buffer amplifier mounted in casing.

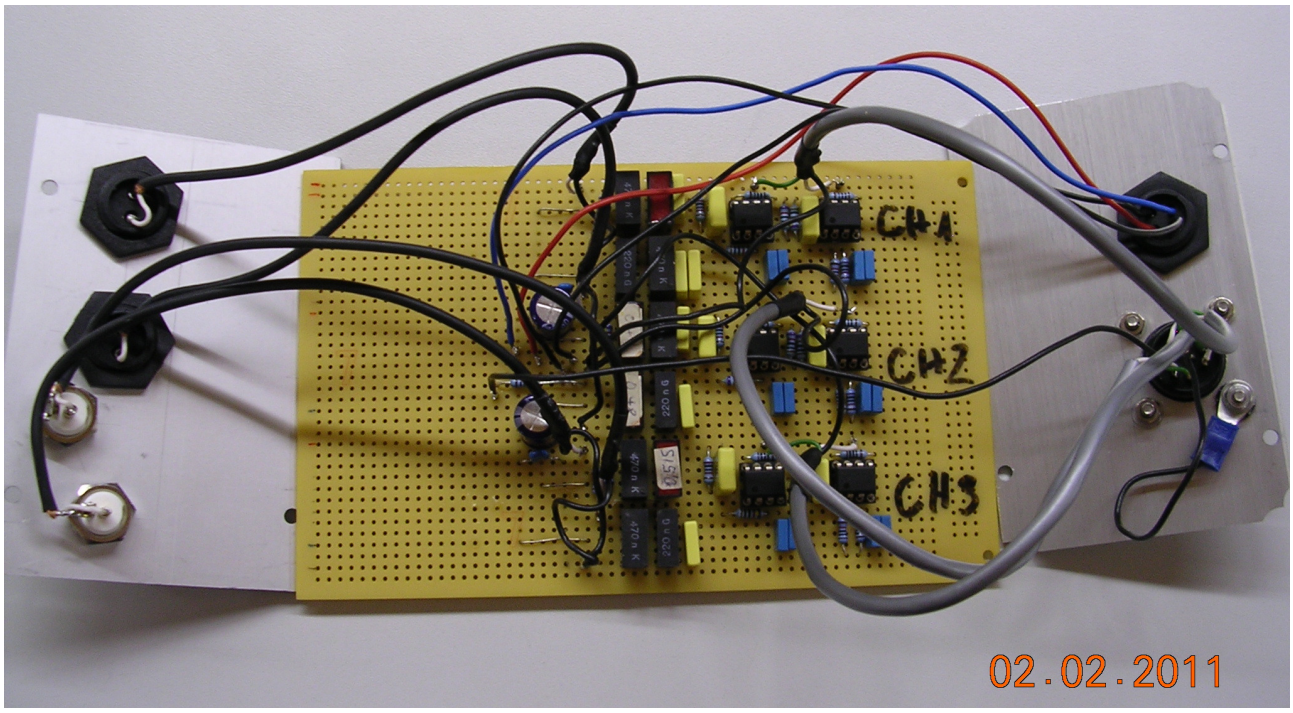

Figure 8: Picture of buffer amplifier board.

Figure 12: Picture of signal input connectors.

Figure 13: Picture of power supply and signal output connectors.